A New Family of Misfit Layered Oxides with Double Rock Salt Layers Bi$_\alpha$($A_{0.75\pm\varepsilon}$Bi$_{0.25\pm\varepsilon}$O)$_{(3+3x)/2}$$MO_2$ (A = Ca, Sr and M = Co, Cr)

M. Hervieu, Ph. Boullay, C. Michel, A. Maignan, and B. Raveau

Laboratoire CRISMAT, ISMRA-Université de Caen, Boulevard du maréchal Juin, 14050 Caen Cedex, France

A series of Bi-based new misfit layered oxides—Bi$_{0.35}$ (Sr$_{0.74}$Bi$_{0.26}$O)$_{1.72}$CoO$_2$, Bi$_{0.35}$(Ca$_{0.75}$Bi$_{0.25}$O)$_{1.8}$ CoO$_2$, Bi$_{0.08}$Pb$_{0.35}$ (Sr$_{0.68}$Bi$_{0.32}$O)$_{1.62}$CoO$_2$, Bi$_{0.18}$Pb$_{0.4}$(Sr$_{0.76}$Bi$_{0.24}$O)$_{1.74}$CrO$_2$, and Bi$_{0.44}$(Sr$_{0.7}$Bi$_{0.3}$O)$_{1.88}$CrO$_2$—has been synthesized and characterized, using electron microscopy and powder X-ray diffraction. Two sets of reflections are evidenced in the ED patterns, associated to the coexistence of two monoclinic S_1 and S_2 subsystems, with [1 0 0]* and [0 0 1]* as common axes and a parameter misfit along [0 1 0]*: S1 {a, b_1, c, β} with $a \approx 5$ Å, $b_1 \approx 5$ Å, $c \approx 29.8$ Å, and $\beta \approx 93°$ and S_2 {a, b_2, c, β} with $a \approx 5$ Å, $b_2 \approx 2.9$ Å, $c \approx 29.8$ Å, and $\beta \approx 93°$. High-resolution electron microscopy showed that it is the first misfit layered oxides involving double rock salt-type (RS) layers, i.e. triple (AO)-type layers (A = Ca and Sr), with a single (H) hexagonal (CoO$_2$) or (CrO$_2$) layer. As a result, these oxides can be described as the members "$n = 3/m = 1$" of a large family with the general formula Bi$_\alpha$($A_{0.75\pm\varepsilon}$Bi$_{0.25\pm\varepsilon}$O)$_{(n+nx)/2}$(MO$_2$)$_m$. In those structures, the bismuth cations are supposed to be distributed over two sorts of sites: (i) the A-sites, filling partly the RS layers and (ii) the sites located between the RS and the H layers, ensuring the cohesion of the structure. The $\chi(T)$ measurements show a paramagnetic behavior above 100 K and are in agreement with a mixed valence Co^{2+} (high spin) and Co^{3+} (low spin) for all the cobalt oxides. They confirm the presence of Cr^{2+} (high spin) in the chromium phases and evidence strong antiferromagnetic interactions at low temperature and paramagnetism with a Curie–Weiss law above 100 K. The Cr oxides are insulators, whereas the pure Bi–cobalt phases are semiconductors or "dirty" metal when the samples have been lead doped. © 1999 Academic Press

INTRODUCTION

An incredible number of intergrowth compounds, as well for oxides as for chalcogenides, has been discovered these past three decades. Such materials result from the bidimensional matching of two different structures, which allow intergrowth of the latter to be built. In the absence of bidimensional matching, intergrowths of different structures can still be built, but they are more rare, leading to the formation of lamellar composite crystals. In these compounds, usually referred to as misfit layered compounds, the distinct layered subsystems are stacked along a direction normal, or nearly normal, to the layer planes. Since they require the formation of composite crystals, these layered structures are generally characterized by weaker interlayer bonds. In this respect, the misfit layered chalcogenides $(MX)_{1+x}(TX_2)_m$ are fascinating not only for their crystal chemistry, but also for their physical properties (see for review 1–3).

In contrast to chalcogenides, oxides do not display a large number of lamellar composite crystals. The misfit oxides Tl$_\alpha$[(Sr$_{0.9}$O)]$_{1.12}$[CoO$_2$] have been recently synthesized (4). The structure of these oxides consists, like that of the sulfides, of the stacking of single SrO rock salt (RS) type layers with single hexagonal (H) CdI$_2$-type layers; they are the members $m = 1$ of the $(MX)_{1+x}(TX_2)_m$ family. The rock salt-type layers are cation deficient, as observed in several chalcogenides (1, 2). However, in the previous study (4), we suggested that the structures of these oxides differ from that of the corresponding sulfide by the nature of the connection between the RS and H layers. The space located between the RS and H layers is empty in the sulfides, the cohesion being ensured by weak bonds. In Tl$_{0.41}$[(Sr$_{0.9}$O)]$_{1.12}$[CoO$_2$], the structure analysis, with the help of high-resolution electron microscopy (HREM) and EXAFS results, suggested that trivalent Tl exhibits a fourfold coordination and is located in the interlayer space, occupying tetrahedra which are built up from three oxygens belonging to the H layer and one oxygen of the RS layer (Fig. 1). The recent study of the misfit layered cobaltite Tl$_\alpha$[(AO)]$_{1+x}$[CoO$_2$], with A = Ca and Sr (5), shows that both Sr and Ca can be located in the RS layers. The Ca-based misfit oxides, which contain much less thallium ($\alpha < 0.17$), show that the exact distribution of the thallium between the RS layers and the interface sites is so far not completely understood.

The above preliminary investigations suggest that it should be possible to stabilize other misfit layered oxides by varying the nature of the interlayer cation. In this respect, trivalent bismuth is a potential candidate, owing to its $6s^2$ lone pair which favors the formation of lamellar structures.
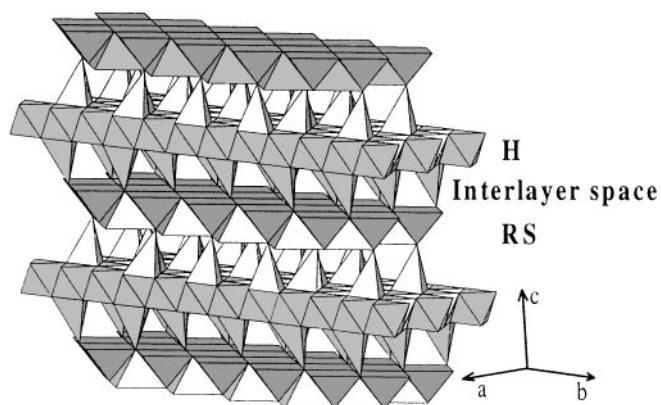
FIG. 1. The misfit layered cobaltite $Tl_x(Sr_{0.9}O)]_{1.12}[CoO_2]$. Perspective view of the structural model. TlO_4 tetrahedra located in the interlayer space are shown.

Moreover, the possibility to replace cobalt by another transition element, such as chromium, should also be considered. In the present paper, we report on the synthesis, structure, and physical properties of the new family of misfit layered oxides $Bi_x(A_{0.75\pm\varepsilon}Bi_{0.25\pm\varepsilon}O)_{(3+3x)/2}(MO_2)$ with $A =$ Ca, Sr and $M =$ Co, Cr. The high-resolution electron microscopy study of these oxides shows that they are, to date, the only misfit layered compounds which contain double RS layers.

EXPERIMENTAL

Synthesis

The systems Bi–Sr–Ca–Co–O and Bi–Sr–Ca–Cr–O were systematically investigated, following the general formula $Bi_x[(AO)]_yMO_2$ with $A =$ Ca or Sr and $M =$ Co or Cr, varying α between 0.5 and 1.2 and y from 1.1 to 2.

A precursor was first synthesized, using the Sr and/or Ca carbonate and the cobalt oxide Co_3O_4 or the chromium oxide Cr_2O_3. Pb doping was also attempted. The precursors were weighted according to the above formulation, i.e., y mol of Sr or Ca carbonate for 1/3 mol of Co_3O_4 or for 1/3 mol of Cr_2O_3 and 1/3 Cr^0, and finely ground. They were heated at 950°C, for a complete decarbonation (about 24 h). The bismuth oxide, $\alpha/2$ mol of Bi_2O_3, or a mixture of Bi_2O_3 and PbO for the doped oxides, was then added. The mixture was pressed in the form of bars, sealed in evacuated silica tubes, and heated at 850°C. The Cr-based compounds were also synthesized, starting from Cr_2O_3 and working under N_2 flow, at the same temperature. The first experiments were carried out, scanning widely the α and y ranges. These samples were analyzed. The A/Co and A/Cr ratios range between 1.25 and 1.35, whatever the nominal composition, whereas the Bi/M ($M =$ Co and Cr) ratio varies over a rather large domain, with $0.7 \leq$ Bi/Co ≤ 0.9 and

$0.8 \leq$ Bi/Cr ≤ 1.1. A second series of samples was then synthesized on the basis of these results.

Structural Investigation

The electron diffraction (ED) study was carried out using a JEOL 200 CX electron microscope fitted with an eucentric goniometer ($\pm 60°$). The HREM was performed with a TOPCON 002B operating at 200 kV (point resolution of 1.8 Å). HREM image calculations were carried out with the Mac-Tempas multislice program. The two microscopes are equipped with EDS analysers.

The powder X-ray diffraction (XRD) data were collected with a Philips vertical diffractometer ($CuK\alpha$ radiation) in the range $5° < 2\theta < 100°$ by increment of $0.02°$ (2θ). Cell parameter calculations were performed by profile analysis (program Fullprof version 3.2, using the profile matching option) (6).

Magnetic and Electrical Characterization

Magnetization measurements were performed from 5 to 400 K, in 0.3 T, after zero field cooling using a SQUID magnetometer.

Resistivity was measured during cooling, from 300 to 5 K, on sintered bars with dimensions $0.2 \times 0.2 \times 1$ cm^3, using a standard four-probe method.

RESULTS

For the above thermal process, six new isotypic phases are isolated. The cationic compositions of these oxides, determined by EDS analysis carried out on about 30 crystallites per sample, are listed in Table 1. The cobalt oxides are black, whereas the chromium compounds are brown. Note that these oxides exhibit a molar A/M ratio ($A =$ Ca, Sr and $M =$ Co, Cr) significantly higher than 1, i.e., much larger than that observed for the $m = 1$ members of the misfit layered sulfides $(A)_{1+x}(TX)_2$ and of the misfit layered oxides $Tl_x(A_{1-\delta}O)_{1+x}CoO_2$.

Electron and X-ray Diffraction

The reconstruction of the reciprocal space from ED patterns of twin free crystallites shows that each of the new phases is characterized by the coexistence of two monoclinic subsystems, with [1 0 0]* and [0 0 1]* as common axes and a parameter misfit along [0 1 0]*. The intense reflections are indexed in the following subsystems:

$$S_1\{a, b_1, c, \beta\} \quad \text{with } a \approx 5 \text{ Å}, b_1 \approx 5 \text{ Å}, c \approx 29.8 \text{ Å},$$
$$\text{and } \beta \approx 93°$$

TABLE 1
Analytical Results and Crystal Data for the Misfit Layered Oxides, $Bi_z[(AO)_{(3+3x)/2}][MO_2]$

EDS average composition	S$_1$				S$_2$	Average	
	a (Å) (± 0.005)	b_1 (Å) (± 0.05)	c (Å) (± 0.02)	β (°) (± 0.03)	b_2 (Å) (± 0.005)	b_1/b_2	m/p
$Bi_{0.8}Sr_{1.35}Co$	4.923	5.118	29.780	92.98	2.832	1.81	8/5
$Bi_{0.8}Sr_{1.27}Co$	4.841	4.935	29.769	92.50	2.829	1.74	7/4
$Bi_{0.6}Pb_{0.35}Sr_{1.1}Co$	4.927	5.204	30.057	92.70	2.815	1.85	11/6
$Bi_{0.8}Ca_{1.35}Co$	4.974	4.723	29.334	93.49	2.810	1.67	5/3
$Bi_{0.6}Pb_{0.4}Sr_{1.32}Cr$	5.165	4.872	30.417	93.72	2.818	1.72	12/7
$Bi_1Ca_{1.32}Cr$	5.070	4.486	29.646	93.09	2.809	1.60	8/5

Note. $a_2 = a_1$, $c = c_1$, $b_2 = b_1$.

$$S_2\{a, b_2, c, \beta\} \quad \text{with } a \approx 5 \text{ Å}, b_2 \approx 2.9 \text{ Å}, c \approx 29.8 \text{ Å},$$

$$\text{and } \beta \approx 93°.$$

The two subsystems of reflections [0 0 1], indexed with suffixes 1 and 2, are clearly observed in the ED patterns of untwinned microcrystals of "BiSrCo" (Fig. 2a), "BiCaCo" (Fig. 2b), "BiSrCr" (Fig. 2c), and "BiCaCr" (Fig. 2d). A $[1\,1\,0]_1$ pattern is given in Fig. 3a.

The a and b_1 parameters are correlated to the "a_c" parameter of the cubic rock salt structure ($a \approx b_1 \approx a_c$), whereas the a and b_2 are correlated to the "a_H" parameter of the hexagonal structure of CdI$_2$-type ($a \approx a_H\sqrt{3}$, $b_2 \approx a_H$). The a, b_1, b_2 parameters are thus similar to those observed for the Tl-based compounds $Tl_z(A_{1-\delta}O)_{1+x}CoO_2$ (4, 5). In contrast, the $c \approx 29.8$ Å and $b \approx 93°$ values show that the stacking sequence of the layers along a is different from that observed in the $m = 1$ misfit layered oxides $Tl_z(A_{1-\delta}O)_{1+x}CoO_2$, in agreement with the different composition of these new phases which contain an excess of A cations with respect to the thallium cobaltites. The conditions limiting the intense reflections, hk_20 ($h + k_2 = 2n$), for the S_2 subsystem, are similar to those observed for the thallium misfit layered cobaltite. In contrast, the conditions on the intense reflections, hk_10 ($h, k_1 = 2n$) are those of a distorted F-type lattice; they are different from those observed for the Tl misfit oxides, giving a confirmation of the lattice change. However, in this S_1 system, there systematically exist weak extra reflections which show that the lattice is actually P-type. For example, in the [0 0 1] ED patterns recorded for "Bi$_{0.8}$Sr$_{1.35}$Co" and "Bi$_{0.8}$Ca$_{1.35}$Co" oxides, the $0\,1\,0_1$, $1\,1\,0_1$, and $1\,0\,0_1$ reflections are clearly observed (see arrows in Figs. 2a and 2b).

In all these compounds, the b_1/b_2 ratios are incommensurate, they depend on the nature of the A and M cations and on the actual composition of the crystallites. The b_1/b_2

values are given in Table 1, as well as the closer ratio of integral number (m/p).

The XRD powder patterns of these oxides corroborate the ED observations. As illustrated for the "Bi$_{0.8}$Ca$_{1.35}$Co" oxide in Fig. 4, it must be emphasized that the reflections corresponding to the S_2 subsystem are weaker. Nevertheless the cell parameters of the two systems were refined with starting values determined from ED patterns; they are given in Table 1. In all these systems, the Ca for Sr substitution involves a strong decrease of the b_1 parameter, in agreement with the size of the two cations, whereas the b_2 parameter remains rather unchanged. An inversion of the a/b_1 ratio in the S_1 subsystem parameters is also observed for the cobalt oxides, with $a/b_1 > 1$ for the Sr-based compounds and $a/b_1 < 1$ for the Ca-based compounds. A similar double evolution was observed in the $Tl_z[(Sr_{1-y}Ca_yO)_{1+x}][CoO_2]$ oxides (5), with a pseudo-tetragonal RS system for $y = 0.25$. Due to excess number of variables with regard to the number of informations and the composite nature of the samples, no structure calculations can be carried out from XRD data.

It is worth pointing out that numerous [0 0 1] ED patterns evidence the formation of twinning domains. These patterns are complex because different types of variants are commonly superposed: three variants of the S_1 system associated to twinning by the S_2 system (they are 60° oriented) and two variants associated to twinning by the S_1 system (they are 90° oriented). Such a phenomenon results from the distortion of the two subsystems and is favored by the existence of weak bonds in the structure. One example of [0 0 1] ED pattern recorded for a twinned crystallite of the "Bi$_{0.8}$ Sr$_{1.35}$Co" oxide is given in Fig. 3b; the three variants, 60° oriented, of the S_1 system are observed, they are denoted by the suffixes I, II, and III. Finally, we notice another phenomenon that is the existence of weak diffuse streaks, often observed along c^*, especially for the "Bi$_{0.8}$Sr$_{1.35}$Co"

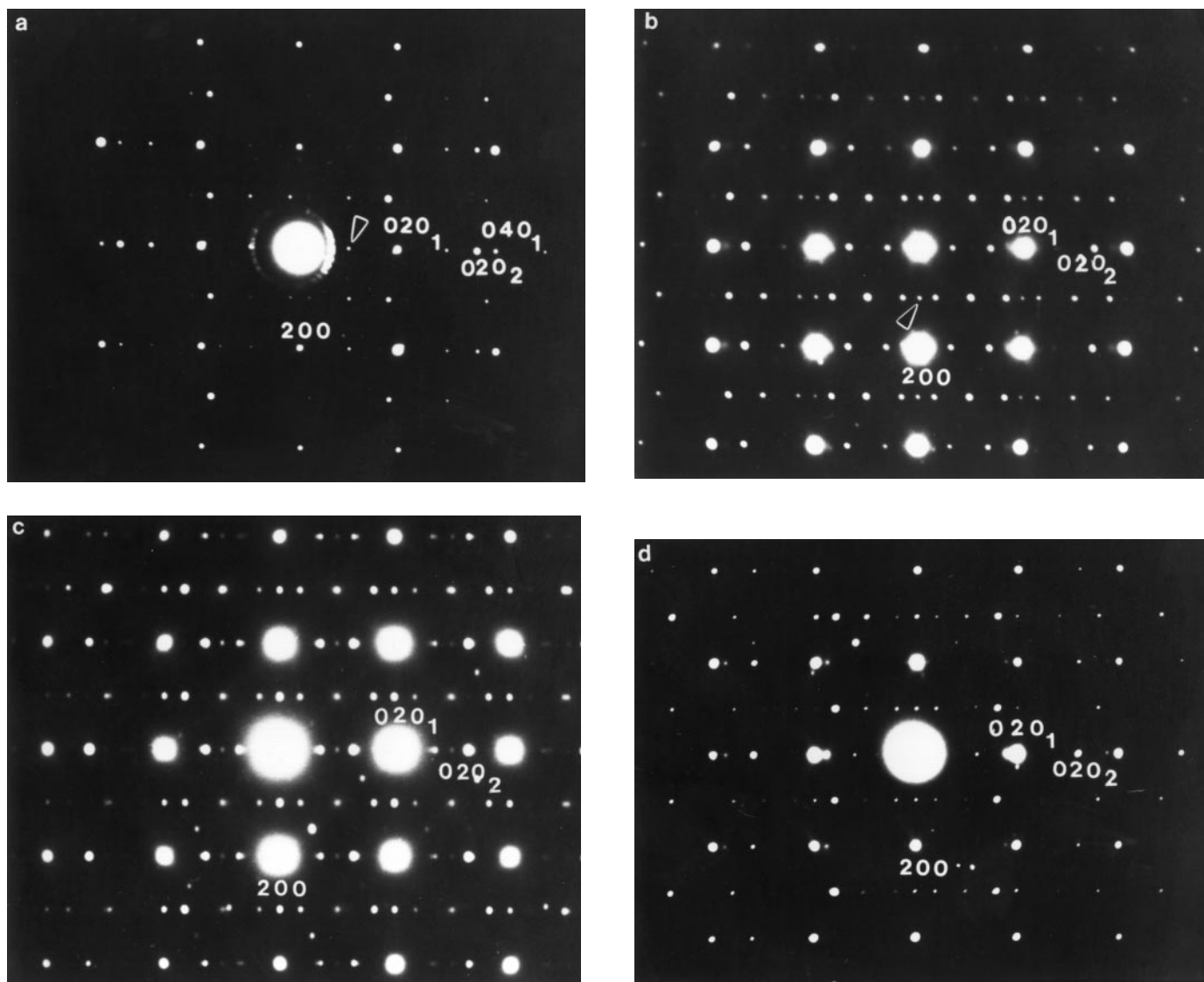**FIG. 2.** [0 0 1] ED patterns of the (a) $Bi_{0.8}Sr_{1.35}Co$, (b) $Bi_{0.8}Ca_{1.35}Co$, (c) $Bi_{0.6}Pb_{0.4}Sr_{1.32}Cr$, and (d) $Bi_1Ca_{1.32}Cr$ phases. The suffixes characterize the first and second systems and the arrowheads show reflections which indicate that the actual lattice is P-type.

oxides. This effect is coupled with twinning as shown from the [0 1 0] ED pattern given in Fig. 3c (the two arrows show the two sets of reflections due to the superposition of the two variants). The corresponding images (see further) show that this feature is not generated by stacking defects, but, likely, by local distortions and atomic disorder at the level of the rock salt-type layers.

HREM Study: A Structural Model for the Misfit Layered Cobaltite $Bi_{0.35}(Sr_{0.74}Bi_{0.26}O)_{1.72}CoO_2$ and $Bi_{0.35}[Ca_{0.75}Bi_{0.25}O]_{1.8}CoO_2$

In order to identify the different kinds of layers stacked along c, the '$Bi_{0.8}Sr_{1.27}Co$' and "$Bi_{0.8}Ca_{1.35}Co$" oxides

were investigated by high-resolution electron microscopy. The interpretation of the contrast was made by the comparison of images with those recorded for the sulfides (9), the Tl-based misfits $Tl_z[(AO)_{1+x}[CoO_2]$ (4, 5), and, for $[1 1 0]_1$ images, with the help of images recorded for different rock salt-related compounds (see for example Ref. (7) for a double rock salt-type layer and Ref. (8) for a triple RS layer). Theoretical images were calculated using the ideal positions calculated from ideal models which were proposed from the ED, XRD, and HREM information. They were calculated for commensurate "supercells," i.e., considering the integral values of m and p given in Table 1 (7/4 for the "$Bi_{0.8}Sr_{1.27}Co$" oxide and 5/3 for "$Bi_{0.8}Ca_{1.35}Co$"); they are detailed further.
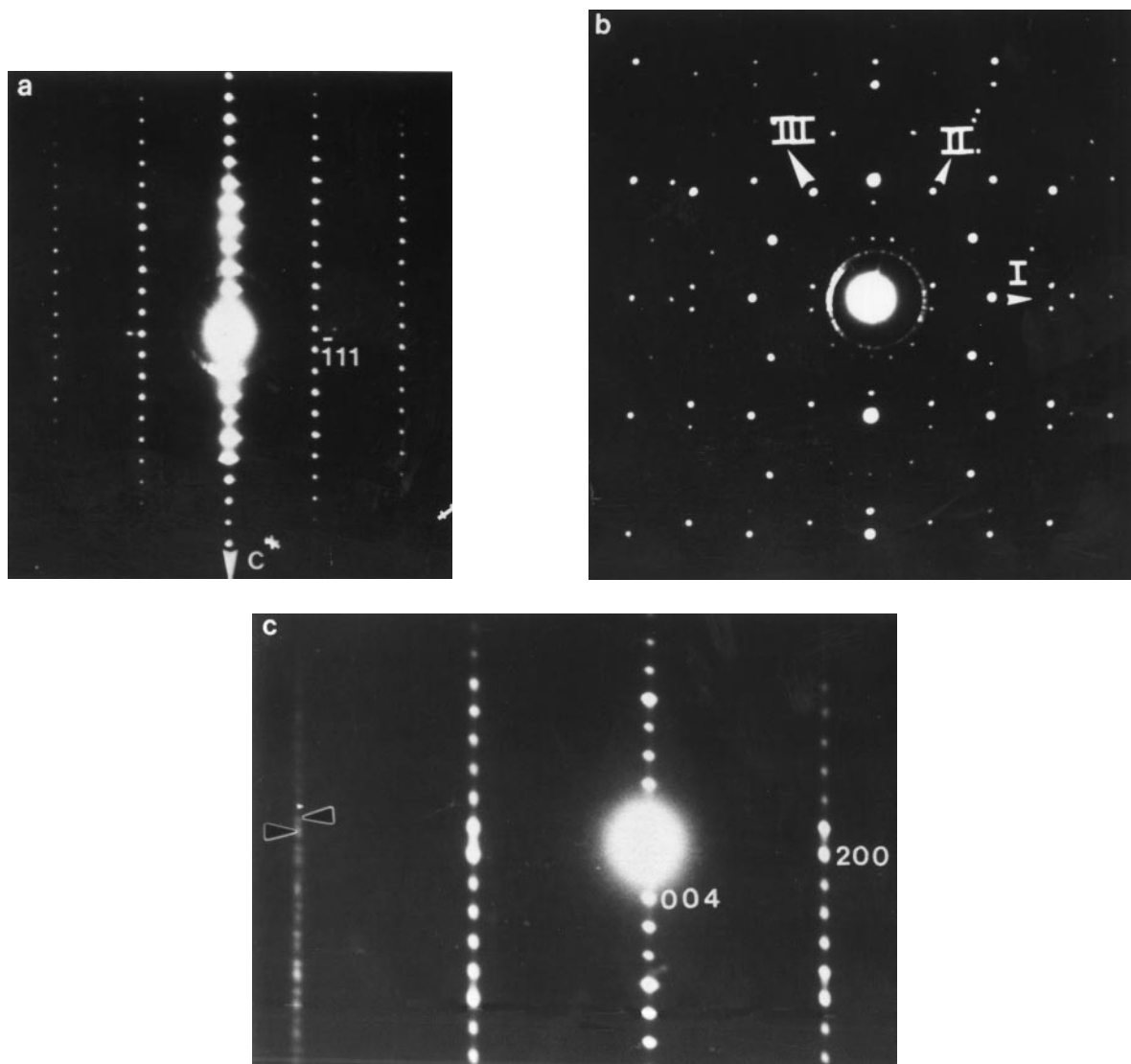
FIG. 3. $Bi_{0.8}Sr_{1.27}Co$ cobaltite. (a) $[1\,1\,0]_1$ pattern and (b) example of $[0\,0\,1]$ pattern of a crystal in which the three variants (denoted I, II, and III), $60°$ oriented, are superimposed (to be compared to Fig. 2a). (c) $[0\,1\,0]$ pattern. Second type of twinning phenomenon observed in the misfit layered Bi-based oxides.

In order to identify the different $(0\,0\,1)$ layers, the structure should be explored by HREM along a direction perpendicular to c. The variation of the c parameter and the excess of A cations $(A = Sr, Ca)$ suggest that the nature of the rock salt layer has changed; at least they are thicker than in the misfit layered oxide $Tl_x[Sr_{0.9}O]_{1+x}CoO_2$ (4, 5).

The numerous images, recorded along $[h\,k\,0]$ for the four samples, show a common characteristic which is the high regularity of the layer stacking mode along the c axis. No intergrowth defect was detected. This is illustrated in Fig. 5, which is an enlarged part of an overall image of the "$Bi_{0.8}Sr_{1.35}Co$" cobaltite.

The $[1\,1\,0]_1$ direction is attractive for viewing the crystal since it should make it possible to image the way the atoms are distributed at the level of the rock salt layers: it was preferentially selected. These images show that the stacking mode is the same for the four oxides. In the $[1\,1\,0]_1$ enlarged image, recorded for the "$Bi_{0.8}Ca_{1.35}Co$" oxide (Fig. 6a), the heavy electron density zones are highlighted. The main characteristics of the contrast consists of three rows of staggered white dots (indicated by triangles); the white dots are 3.5 Å spaced along $[1\,1\,0]_1$ and each row is spaced by about 3.2 Å. Such a contrast is similar to that observed in oxides whose structure presents rock salt-type layers; in the present compounds, it is associated to three adjacent $[CaO]_\infty$ (or $[SrO]_\infty$) layers, which form a double rock salt-type layer. Each group of three $[CaO]_\infty$ layers is shifted along $[1\,\bar{1}\,0]$ with regard to the adjacent ones. Such triple
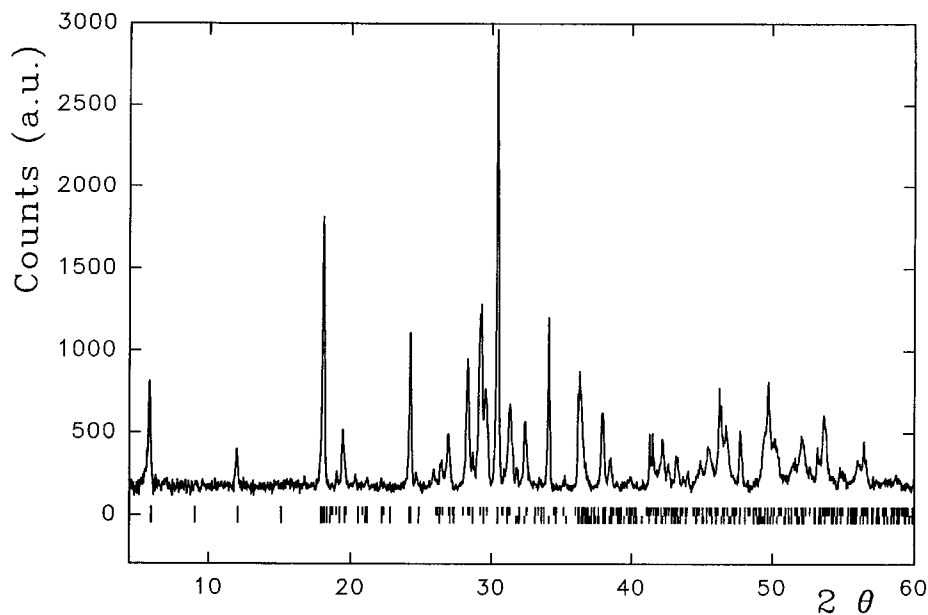
FIG. 4. XRD powder pattern of the $Bi_{0.8}Ca_{1.35}Co$ cobaltite. To limit preferred orientation phenomena, the powder was carefully deposited on grease. Vertical bars correspond to Bragg angle positions for the S_1 subsystem (top bars) and S_2 subsystem (bottom bars).

$[AO]_\infty$ layers are schematized as large black circles in Fig. 6b; the shifting along $[1\bar{1}0]$ between two successive triple layers can easily be seen by considering the medium layer in each group of triple layers. Coming back to the $[110]_1$ HREM image (Fig. 6a), one observes, for this focus value, a dark row and two white rows, rather diffuse. The dark row (denoted Co L) is associated with the presence of a layer of lighter atoms, i.e., to a $[CoO_2]_\infty$ layer as

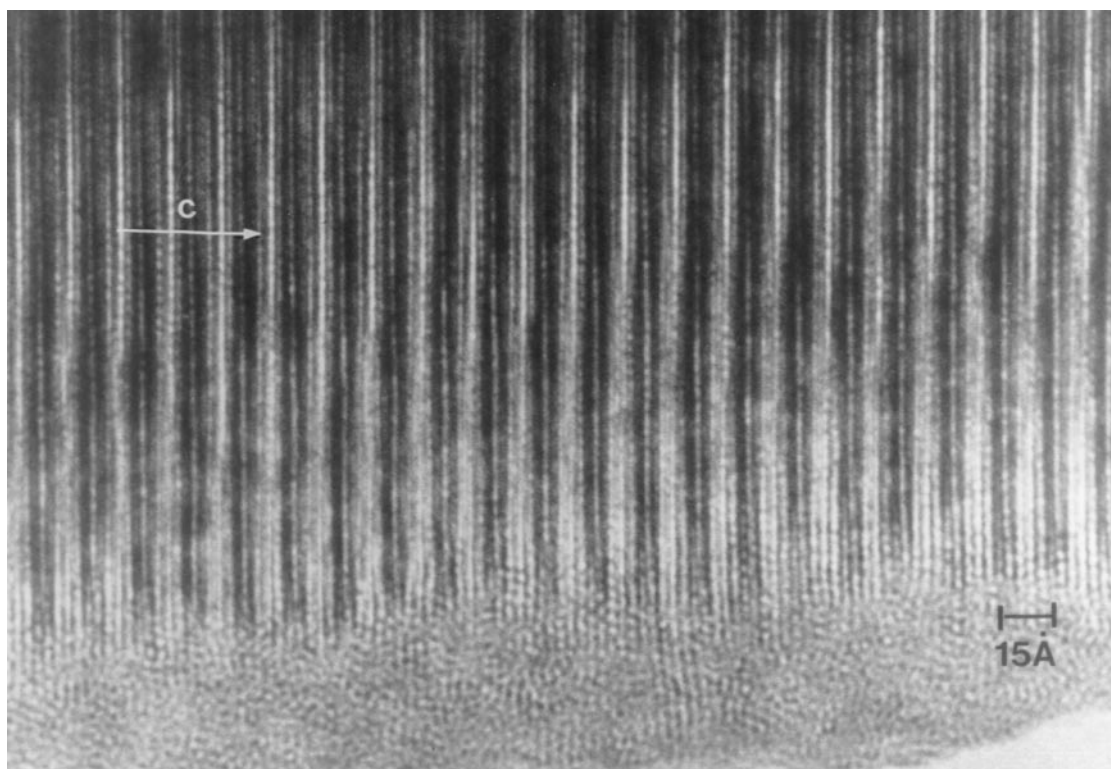**FIG. 5.** Overall image of the "$Bi_{0.8}Sr_{1.35}Co$" cobaltite, showing the high regularity of the layer stacking along c.
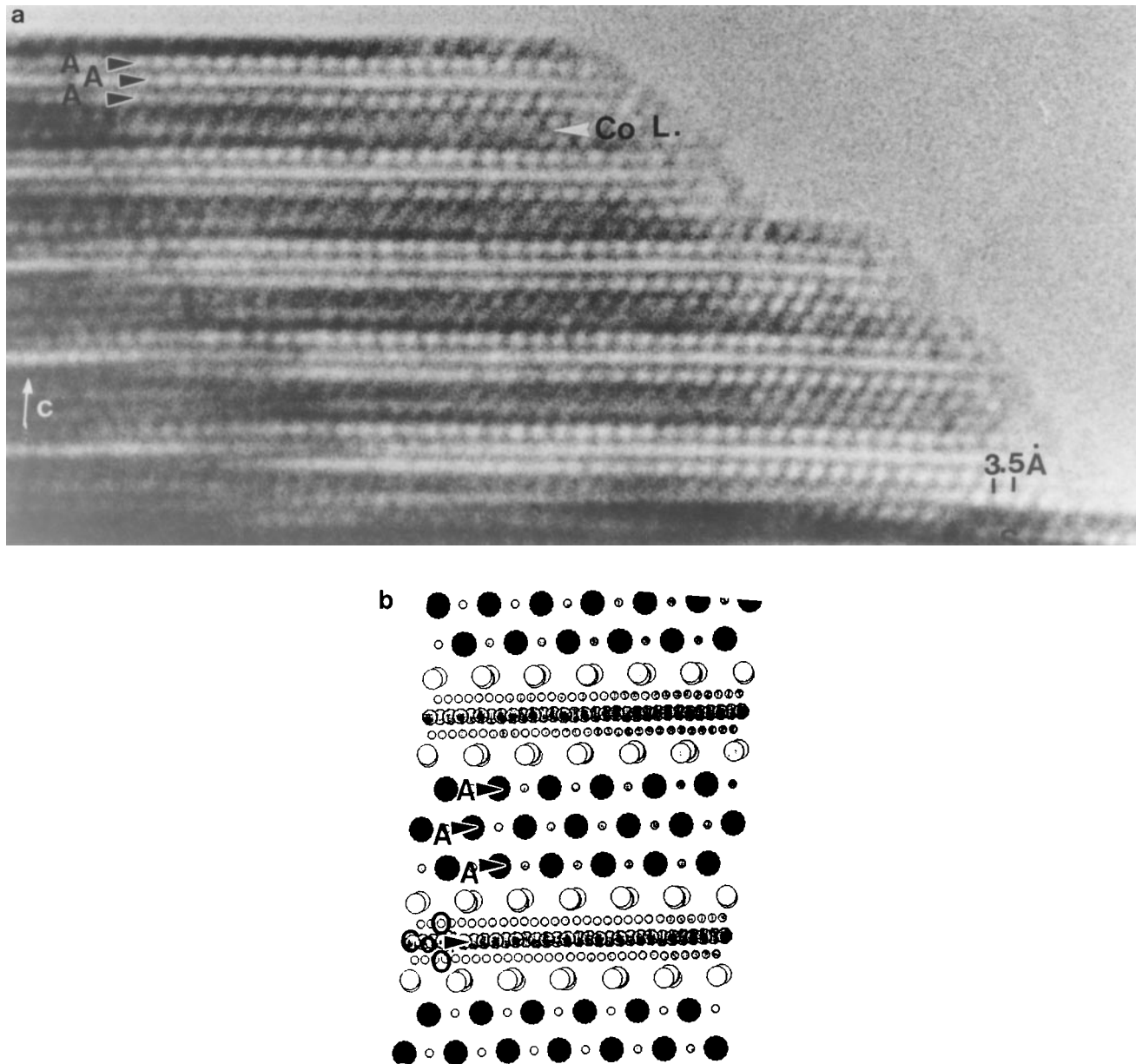
FIG. 6. (a) $[1\,1\,0]_1$ HREM image of the "$Bi_{0.8}Ca_{1.35}Co$" cobaltite. The dots correlated to the A cations of the rock salt layers are indicated by black arrows and the Co layer (Co L) by a white arrow. (b) Projection of the atom columns along that direction (the white circles correspond to the Bi atoms located in the interlayer space).

schematized by the gray smaller circles on Fig. 6b. By comparison with the misfit layered cobaltites $Tl_\alpha[A_{0.9}O]_{1+x}CoO_2$, with $A = Ca$, Sr (4, 5), the diffuse white rows (Fig. 6) are associated to the space separating the $[AO]_\infty$ layers from the $[CoO_2]_\infty$ layers, where at least a part of the bismuth atoms (large white circles in Fig. 6b) are assumed to be located. The problem of the distribution of the Bi layers will be discussed further. In the "$Bi_{0.8}Ca_{1.35}Co$" oxide, the distortion of the rock salt system is more straightforward since the perfect centered array of the white dots in

the three adjacent rows, expected for a RS system, is lost; moreover, the contrast correlated to the positions of the Ca atoms within the intermediate $[CaO]$ layer of the rock salt-slab often becomes blurred. These effects are likely correlated to atomic displacements and twinning phenomena; it is likely responsible of the weak extra reflections and the diffuse streaks along c^* (Fig. 2).

At this point of the investigations a structural model can be proposed for this new misfit layered bismuth cobaltites and chromites (Fig. 7). The latter derives from the Tl based
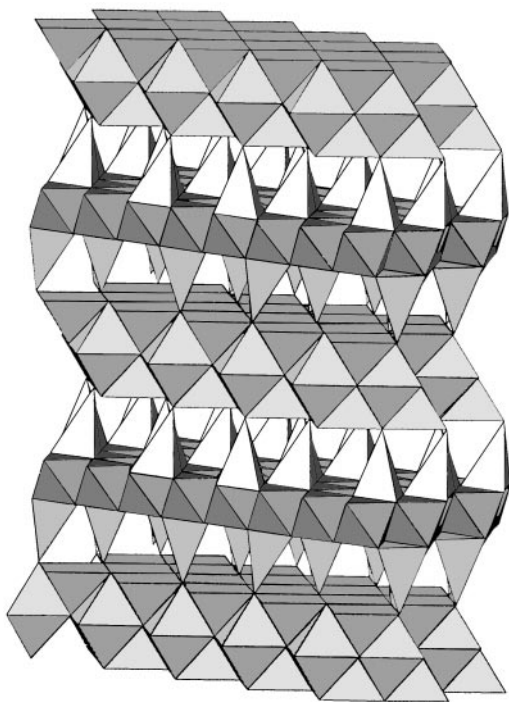
FIG. 7. Structural model for the Bi based misfit layered oxides, $Bi_x[AO]_{(3+3x)/2}[MO_2]$.

misfit cobaltites (4, 5) by the insertion of one additional $[AO]_\infty$ slab at the level of the rock salt-type layer. Thus, the structure of these phases can be described from the stacking of three different layers:

(i) Triple AO slabs, i.e. double rock salt layers (DRS) which generate the first subsystem of reflections S_1. The corresponding lattice is distorted with regard to the ideal cubic RS structure, showing a P-type lattice. The HREM images evidence clearly such DRS layers but show also the distortion of the rock salt-type system, through its monoclinic distortion and through the sometimes elongated shape of the dots correlated to the medium layer of the group of three adjacent $[AO]$ layers. A is mainly Sr or Ca, but the possible partial occupancy of the A-sites by Bi should also be considered (see below).

(ii) Single hexagonal layers (H) generally named CdI2-type layers, but which are in fact $(1\,1\,1)_C$ rock salt-type layers. These layers generate the second subsystem S_2. They are on the nodes of a 2D network with a pseudohexagonal symmetry ($a \approx b_2\sqrt{3}$). Their composition is supposed to be $[CoO_2]$ or $[CrO_2]$. They always appear as a single row of light electron density, i.e., as a dark or a bright row, depending on the focus value.

(iii) An intermediate layer of cations, located between the $[CoO_2]_\infty$ or $[CrO_2]_\infty$ layer and the $[AO]_\infty$ layers, should ensure the cohesion of the structure. The Bi atoms, or a part of the Bi atoms, are supposed to be located in the tetrahedra

built up from three O atoms of the oxygen layer of the hexagonal slice and one O atom of the rock salt layer.

Considering the mismatch parameter, namely $1 + x$, and the formulation adopted for the sulfides and the Tl-based misfit layered compounds, such a stacking mode for these three types of layers would involve a general formulation $Bi_x[AO]_{(3+3x)/2}^{RS}[MO_2]^H$, where A represents the cations located in the rock salt layers and M those of the hexagonal layer.

HREM images were calculated for this theoretical model, varying the focus values and crystal thickness. For these simulations, ideal atomic positions were calculated, taking into consideration the usual interatomic distances in oxides. The supercells used for the calculations are deduced from the m, p values (Table 1), i.e.,

$$a' \approx 4.9 \text{ Å}, \; b' \approx 20.5 \text{ Å} \; (\approx 4b_1 \approx 7b_2) \; c' \approx 29.8 \text{ Å},$$

$$\beta = 92.5° \text{ for the "Bi}_{0.8}Sr_{1.27}Co"$$

oxide and $a' \approx 4.9$ Å, $b' \approx 14.6$ Å ($\approx 3b_1 \approx 5b_2$) $c' \approx 29.3$ Å,

$$\beta = 93.5° \text{ for the "Bi}_{0.8}Ca_{1.35}Co" \text{ oxide.}$$

According to the above description of the layers, three different limit structural distributions of the cations were tested for the image simulations in "$Bi_{0.8}Ca_{1.35}Co$" oxide.

(I) Full occupancy of the H layers by cobalt, of the RS layers by calcium and bismuth, and partial occupancy of the interlayer space by bismuth according to the formula $Bi_{0.35}[(Ca_{0.75}Bi_{0.25}O)_{1.8}]^{RS}[CoO_2]^H$.

(II) Full occupancy of the H layers by cobalt, distribution of calcium in the RS layer which is then cation deficient, bismuth being located in the interlayer space only, according to the formula $Bi_{0.8}[(Ca_{0.75}\square_{0.25}O)_{1.8}]^{RS}[CoO_2]^H$.

(III) Full occupancy of the RS layers by calcium and bismuth, distribution of the remaining bismuth in the H layers together with cobalt, partial occupancy of the interlayer space by cobalt, according to the formula $Co_{0.35}[Ca_{0.75}Bi_{0.25}O)_{1.8}]^{RS}[Co_{0.65}Bi_{0.35}O_2]^H$.

Considering these three models, the [3 1 0] and [0 0 1] HREM images were calculated for the through focus series, varying the crystal thickness. These models correspond to the same ideal atom coordinates, calculated for the model proposed in Fig. 8 (space group $P2_1/m$); they only differ by the Bi and Ca distribution within the interlayer space and the rock salt layers. For the latter, a statistical distribution of Bi and Ca was taken into consideration in the models I and III.

Four selected images, calculated for four focus values ($\Delta f = 0$, -250, -500, and -750 Å) and three interlayer space occupancies (Bi content = 1, 0.5, and 0) are given in Fig. 8a. The variation of contrast, at the level of the interlayer space, vs the Bi content is clearly observed; for
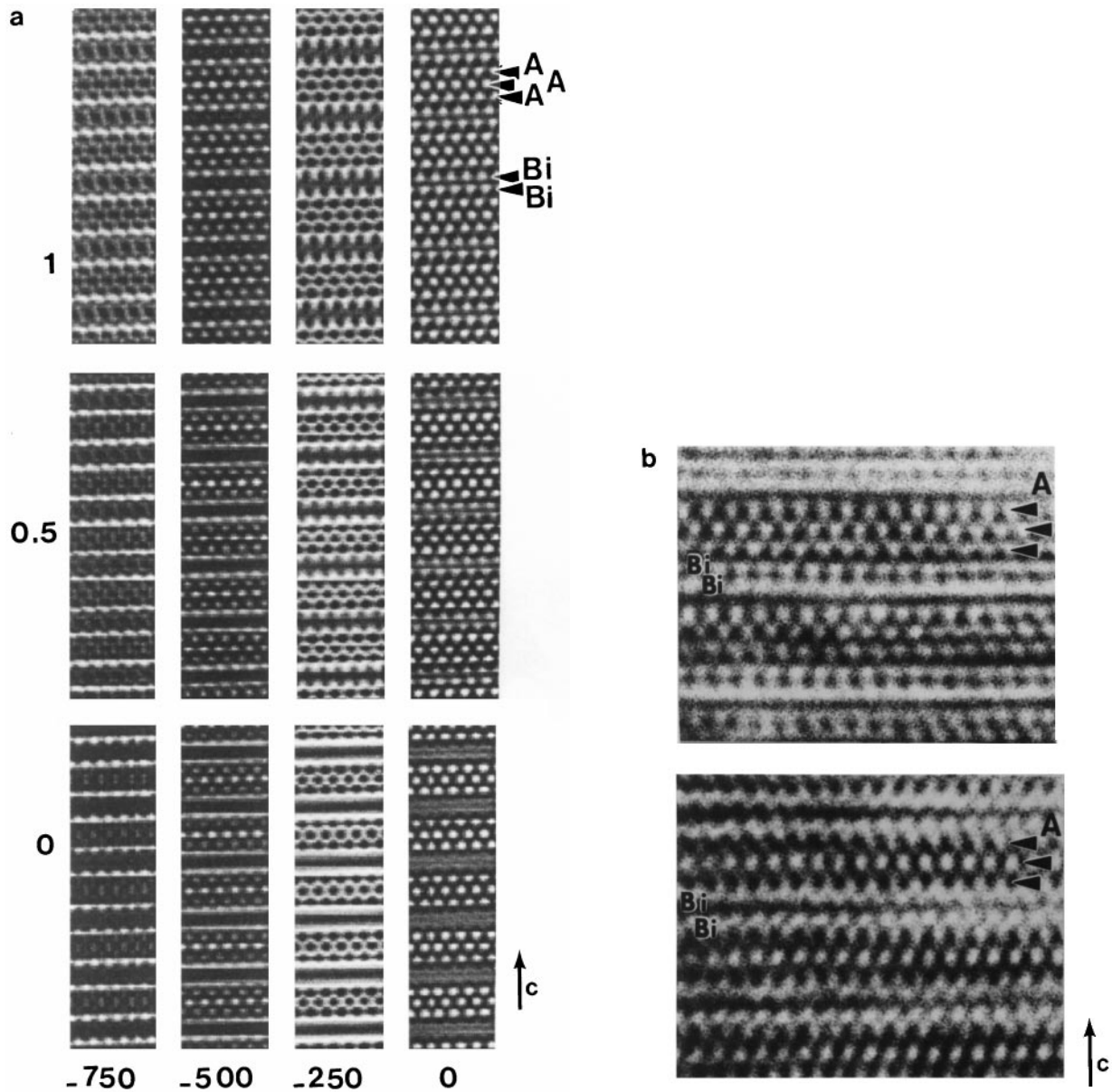
FIG. 8. (a) Calculated $[1\,1\,0]_1$ images for the $Bi_{0.8}Ca_{1.35}Co$ cobaltite, according to three occupancy factors for Bi in the interlayer space. The focus values are -750, -500, -250, and 0 Å and the considered occupancies are 1 (the sites are fully occupied), 0.5 (half occupancy), and 0 (the sites are empty). Crystal thickness ≈ 25 Å. (b) Experimental images.

example for the three first Δf values (close to 0, -250, and -500 Å) a full occupancy of these sites involves the formation of very bright dots, whereas for empty sites, the contrast is weak and blurred. For a few focus values (such as -750 Å), the difference in contrast is not straightforward. Two significant experimental images, where the heavy electron density corresponds to bright and dark dots, respectively (close to 0 and -250 Å), are compared in Figs. 8b. At the level of the interlayer space (indicated by the symbol Bi), bright (for $\Delta f \approx 0$ Å) or dark (for $\Delta f = -250$ Å) dots are clearly observed, indicating that Bi atoms are located at this

level; however, comparing the brightness or darkness of these dots, with the theoretical images obtained for fully occupied and empty interlayer space (Fig. 8a), show that the best fit is in fact obtained for a partial occupancy, in favor of the distribution (I). This suggests that the bismuth sites are only partly occupied and, therefore, that some of the calcium sites are occupied by bismuth. In the case of the "$Bi_{0.8}Sr_{1.35}Co$" oxide, a similar agreement between the calculated an observed HREM images is obtained so that this compound should also be formulated on the same way $Bi_{0.47}[Sr_{0.8}Bi_{0.2}O)_{1.66}]^{RS}CoO_2$.

The main contrast of the $[0\,0\,1]_{1,2}$ HREM images of these oxides (as shown in the enlarged image in Fig. 9a recorded for the "$Bi_{0.8}Ca_{1.35}Co$" oxide) is an array of white spots, spaced by 2.5 Å; this contrast is similar to that observed for the Tl-based oxides (4, 5) and also for the sulfides (8). This array is the signature of the rock salt layer, whereas the H layer is scarcely visible. The modulation of this contrast with sequences of brighter and less bright dots is the signature of the misfit character:

— In the "$Bi_{0.8}Sr_{1.35}Co$" oxide, the sequence is three brighter dots which alternate with five less bright dots, along b, following an average periodicity of 20.5 Å (Fig. 9b). The alternation is shifted by 20.5/2 Å in the adjacent row, involving a centered contrast. This periodicity corresponds to the commensurate supercell approximation, considering the closest common multiple of the b_1 and b_2 parameters ($b \approx 7 \times b_2$ and $4 \times b_1$). The images calculated for a supercell which would exhibit the $b_1/b_2 = 7/4$ ratio confirm this interpretation. However, b_1/b_2 deviates slightly from 7/4, so that the misfit between the two networks and the incommensurate character of the superposition generates deviations from this "ideal" alternation of three bright and five less bright dots; two or four adjacent bright dots, instead of three, are in fact often observed. As previously mentioned in the Tl compounds (4, 5), the presence of cations in the interlayer space is hardly visible in the Sr based compounds; the problem is indeed amplified in the Bi–Sr-based misfit since there is an additional [SrO] layer.
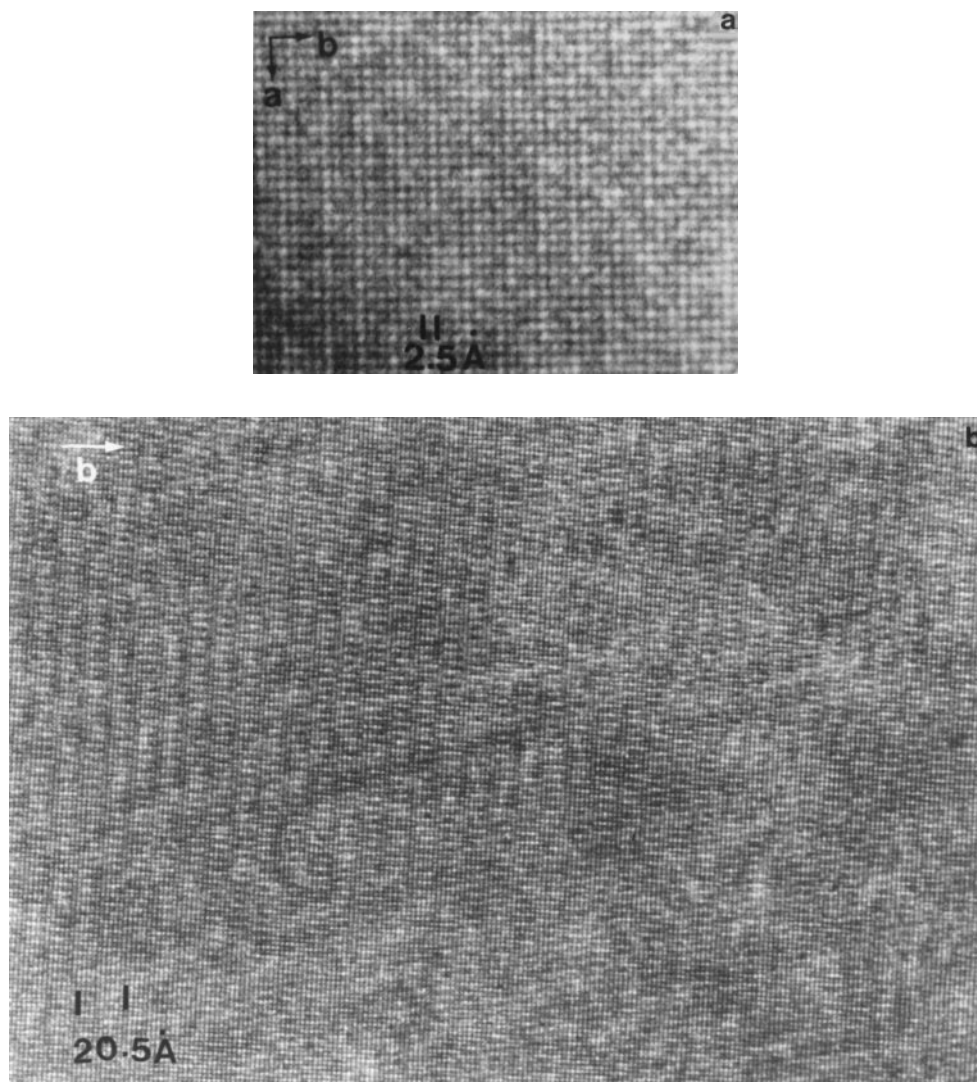

FIG. 9. $[0\,0\,1]$ HREM images. (a) Enlarged image showing the square array of bright dots. (b) Overall image of the $Bi_{0.8}Sr_{1.35}Co$ cobaltite, with a periodicity along b which is close to 20.5 Å and (c) of the $Bi_{0.8}Ca_{1.35}Co$ cobaltite, periodicity along b close to 14.6 Å. (d) Calculated images for the different distributions in the $Bi_{0.8}Ca_{1.35}Co$ cobaltite (focus values of -250 and -500 Å). Crystal thickness ≈ 25 Å.

-250Å -500Å

Bi0.35(Ca0.75Bio.25)1.8(CoO2)

Bi0.8(Ca0.75O)1.8(CoO2)
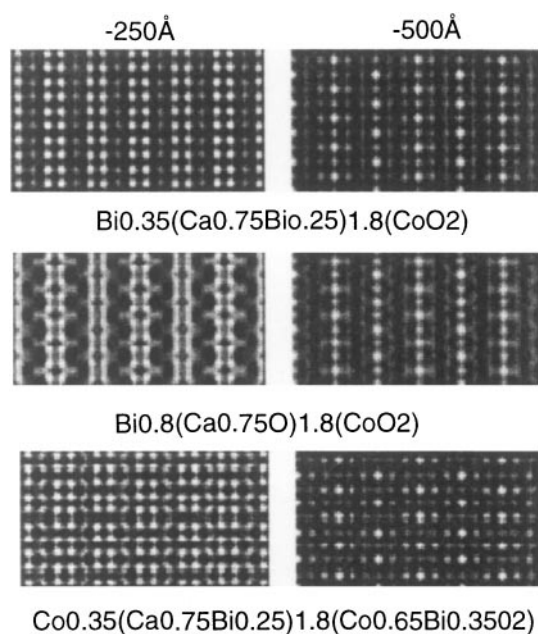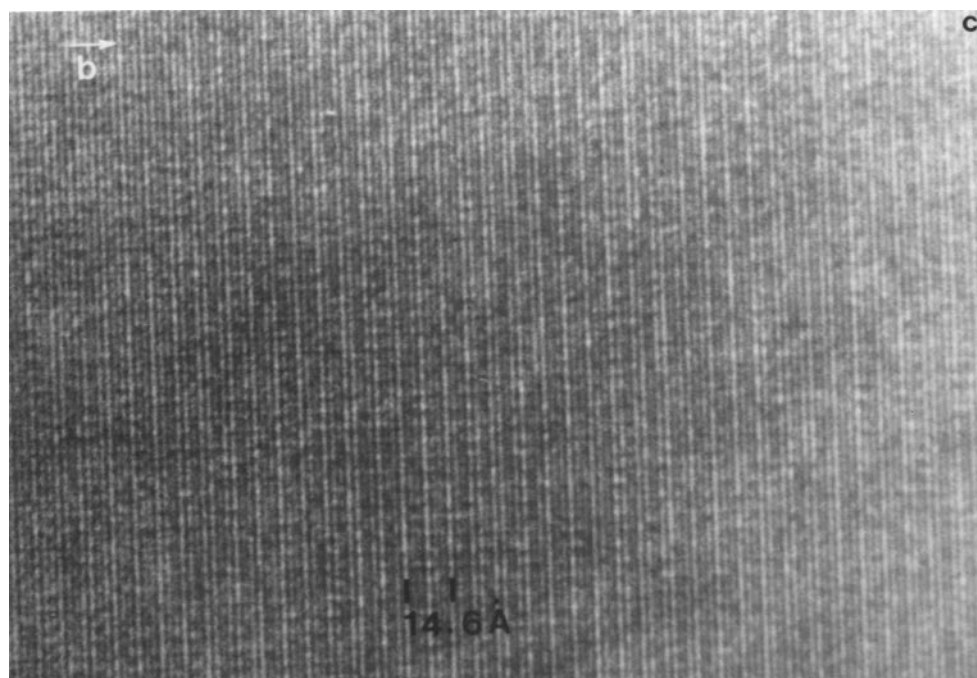
Co0.35(Ca0.75Bi0.25)1.8(Co0.65Bi0.3502)

FIG. 9—*Continued*

— In the "$Bi_{0.8}Ca_{1.35}Co$" oxide, the lower scattering factor of Ca with regard to Bi makes it possible to enhance the contrast. This is illustrated in Fig. 9c: the modulation consists of a sequence of two bright dots and one less bright one. The periodicity along b is close to 14.64 Å ($b \approx 5 \times b_2$ and $3 \times b_1$). The image claculations, carried out for the three above distributions of the cations (Fig. 9d), confirm that the presence of the rows of bright dots parallel to a is correlated

to the presence of the Bi in the interlayer space. The contrast recorded for the distribution I, i.e., $Bi_{0.35}[(Ca_{0.75}Bi_{0.25}O)_{1.8}]^{RS}[CoO_2]^H$, and a focus value close to -250 Å, fits with the experimental image (Fig. 9c).

This HREM study allows a generic formula of these new misfit layered oxides, taking into consideration the fact that the parameter which expresses the mismatch between the RS and H layers ($1 + x/2$) obeys to the relation

$(1 + x/2) = b2/b1$. In these conditions, a large series of co-baltites and chromites, involving alkaline earth cations associated with bismuth, should exist, with the formula $Bi_x[(Sr, Ca, Bi)O]_{(1+x)n/2}[MO_2]_m$ where m is the number of adjacent hexagonal layers, n is the number of adjacent (AO) layers (i.e., $n - 1$ RS layers), $1 + x$ expresses the parameter mismatch and α the cations located within the interlayer space. The ideal structural formula of the present oxides, as well as the corresponding $3(1 + x)/2$ values, deduced from the EDS analysis and from the b_1/b_2 values, are listed in Table 2. All these compounds are the members "$m = 1/n = 3$" of the series with $M = Co$ or Cr.

The accurate structure of these oxides remains to be determined in order to understand the exact cationic distribution. In particular it is not known from this study whether the "AO" layers are perfectly stoichiometric or whether they are cation deficient. Nevertheless, the existence of several oxides in the Bi–Sr–O and Bi–Ca–O systems (10–15), in which Bi^{3+} is associated to Sr and Ca in mixed layers, is in favor of the filling of the RS layer with bismuth. The presence of bismuth in the interlayer spaces, implies for Bi^{3+} a tetrahedral coordination. The latter, although rare, has been observed previously in several oxides, such as $CaBi_2O_4$ (12, 13), $SrBi_2O_4$ (14), and $Ca_6Bi_2O_{15}$ (15). For example, in

$CaBi_2O_4$ (13), Bi^{3+} atoms are fourfold coordinated, in a short distorted pyramid. Nevertheless a possible partial exchange between bismuth and cobalt (or chromium) cannot be ruled out.

Magnetic and Transport Properties

The molar magnetic susceptibility measurements shown in Fig. 10a for two cobalt oxides $Bi_{0.08}Pb_{0.35}$

TABLE 2
The Misfit Layered Oxides $Bi_x[(AO)_{(3+3x)/2}][MO_2]$: Ideal Formulations as Deduced from EDS and b_2/b_1

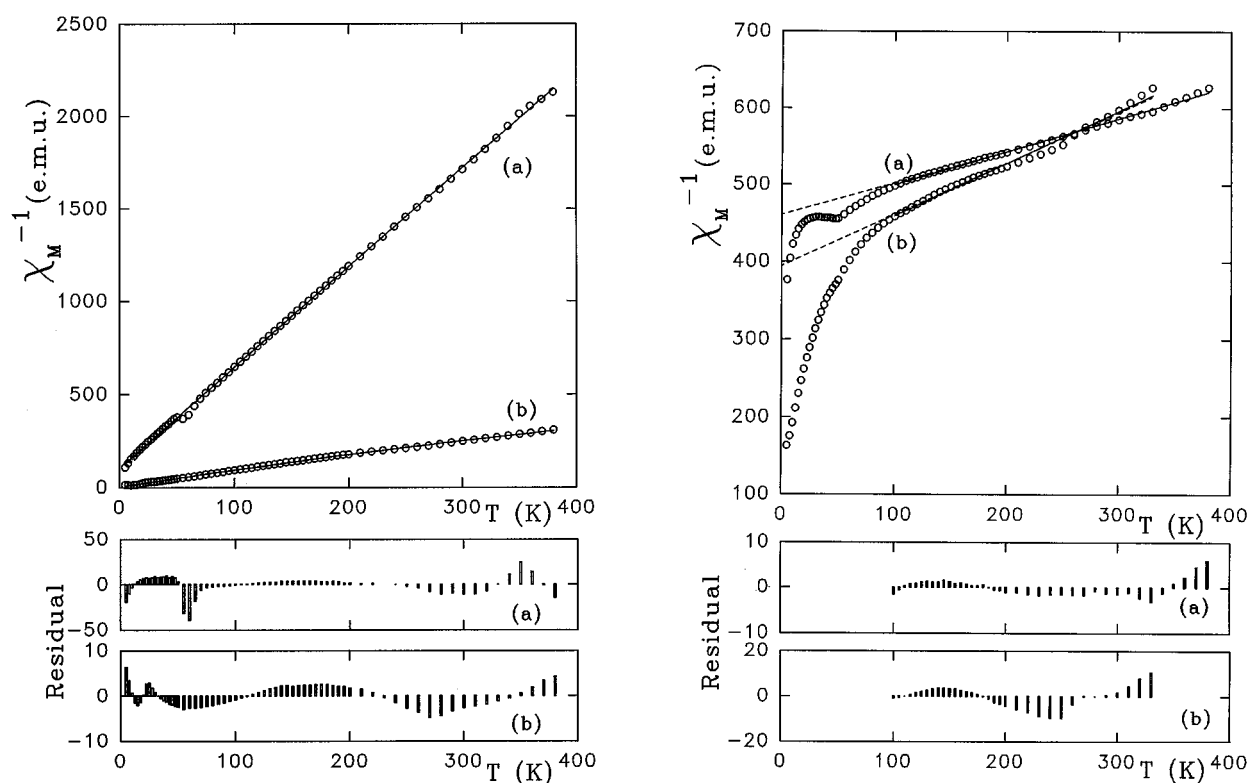| EDS average composition	b_2/b_1	$(3+3x)/2$	$Bi_x[AO]_{(3+3x)/2}[MO_2]$
$Bi_{0.8}Sr_{1.35}Co$	0.55	1.66	$Bi_{0.47}[(Sr_{0.8}Bi_{0.2}O)_{1.66}][CoO_2]$
$Bi_{0.8}Sr_{1.27}Co$	0.575	1.72	$Bi_{0.35}[(Sr_{0.74}Bi_{0.26}O)_{1.72}][CoO_2]$
$Bi_{0.6}Pb_{0.35}Sr_{1.1}Co$	0.54	1.62	$Pb_{0.35}Bi_{0.08}[(Sr_{0.68}Bi_{0.32}O)_{1.62}][CoO_2]$
$Bi_{0.8}Ca_{1.35}Co$	0.60	1.80	$Bi_{0.35}[(Ca_{0.75}Bi_{0.25}O)_{1.8}][CoO_2]$
$Bi_{0.6}Pb_{0.4}Sr_{1.32}Cr$	0.58	1.74	$Bi_{0.18}Pb_{0.4}[Sr_{0.76}Bi_{0.24}O]_{1.74}CrO_2$
$Bi_1Ca_{1.32}Cr$	0.625	1.88	$Bi_{0.44}[(Ca_{0.7}Bi_{0.3}O)_{1.88}][CrO_2]$

FIG. 10. Temperature dependence of the inverse molar magnetic susceptibility (open circles, experimental points; lines, fitted curves, bars, residuals between experimental and calculated values). (a) Cobalt samples: $Bi_{0.08}Pb_{0.35}[Sr_{0.68}Bi_{0.32}O]_{1.62}CoO_2$ (curves a), and $Bi_{0.35}[Ca_{0.75}Bi_{0.25}O]_{1.80}CoO_2$ (curves b). (b) Chromium samples: $Bi_{0.44}[Ca_{0.7}Bi_{0.3}O]_{1.88}CrO_2$ (curves a), and $Bi_{0.18}Pb_{0.4}[Sr_{0.76}Bi_{0.24}O]_{1.74}CrO_2$ (curves b).

$[Sr_{0.74}Bi_{0.26}O]_{1.72}CoO_2$ and $Bi_{0.35}[Ca_{0.75}Bi_{0.25}O]_{1.80}$ CoO_2 show that both of them are paramagnetic. The magnetic susceptibility agrees with a Curie–Weiss law $\chi = \chi_0 + C/(T - \theta)$ with $\theta = -18$ and -2.5 K, respectively. The negative θ value indicates weak antiferromagnetic couplings between cobalt atoms, as observed for the Tl-based series. The observed values of the effective magnetic moment of cobalt (1.13 and 2.85 μ_B) agree well with the

calculated one (1.09 and 2.74 μ_B), taking into consideration the average oxidation states for cobalt deduced from the ideal formula, $+2.9$ and $+2.5$, respectively. Note that the calculations were made, on the basis of a mixture of Co(III) in low spin configuration (0 μ_B) and Co(II) in high spin configuration (3.87 μ_B).

The $\chi^{-1}(T)$ curves of the two chromium oxides, $Bi_{0.18}Pb_{0.4}[Sr_{0.76}Bi_{0.24}O]_{1.74}CrO_2$ and $Bi_{0.44}[Ca_{0.7}$
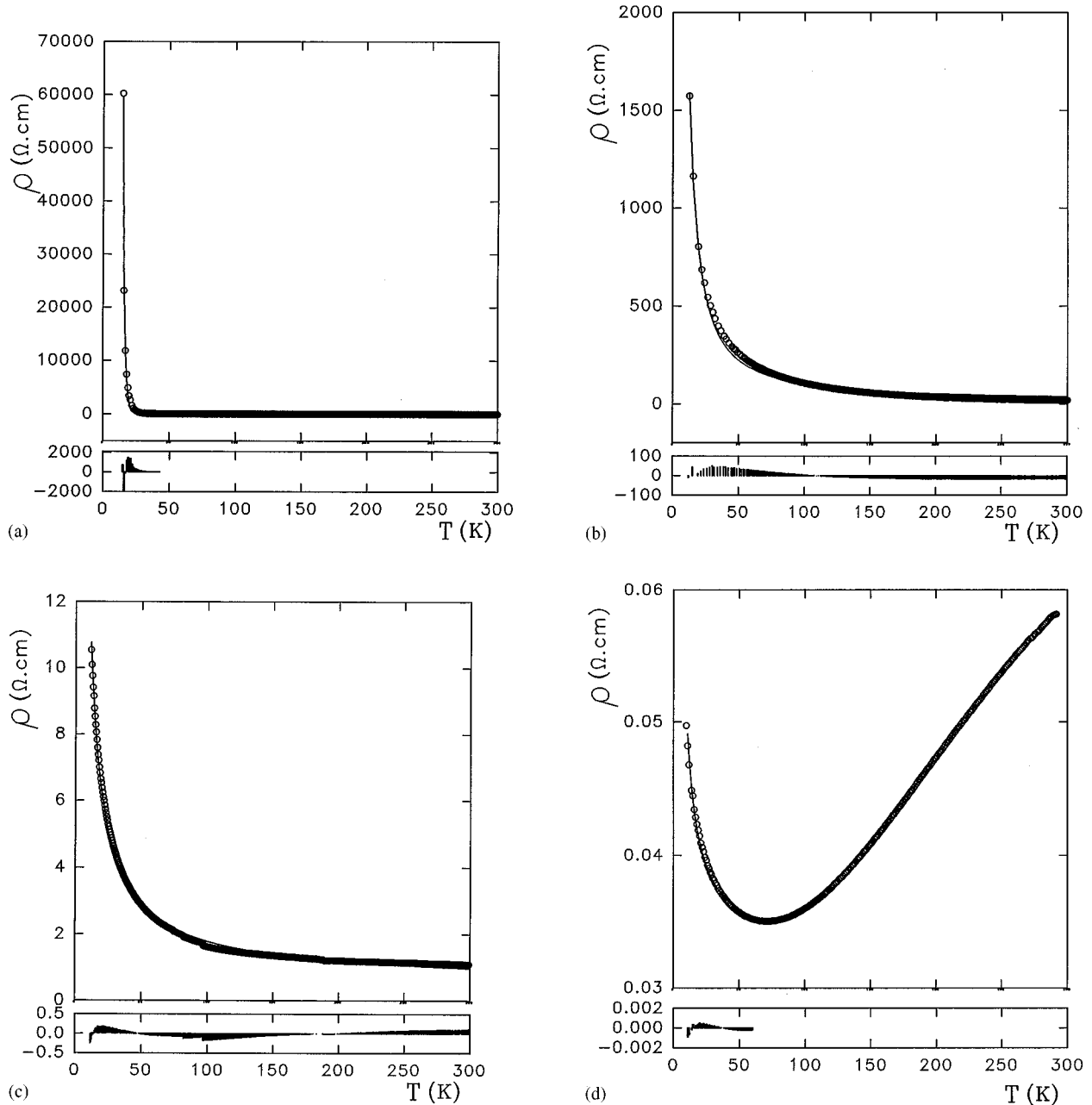

FIG. 11. Temperature dependence of the electrical resistivity for cobalt samples (open circles, experimental points; lines, fitted curves; bars: residuals) for (a) $Bi_{0.35}[Ca_{0.75}Bi_{0.25}O]_{1.80}CoO_2$; (b) $Bi_{0.35}[(Sr_{0.74}Bi_{0.26}O)_{1.72}][CoO_2]$; (c) $Bi_{0.47}[(Sr_{0.8}Bi_{0.2}O)_{1.66}][CoO_2]$; and (d) $Pb_{0.35}Bi_{0.08}$ $[(Sr_{0.68}Bi_{0.32}O)_{1.62}][CoO_2]$.

$Bi_{0.3}O]_{1.88}CrO_2$ (Fig. 10b) evidence strong antiferromagnetic interactions at low temperature, and paramagnetism with a Curie–Weiss law above 100 K. The molar Curie constants, deduced for the high temperature part of the curves, $C = 1.76$ and $C = 2.42$, for the "PbBi" and the "Bi" phases respectively lead to effective magnetic moments of 3.8 and 4.4 μ_B per Cr atom. The formula of the "PbBi" phase implies an average oxidation state of $+2.4$ for Cr, whereas the pure "Bi" should contain only Cr^{2+}. Considering the effective moment of Cr^{3+} (3.9 μ_B) and of high spin Cr^{2+} (4.9 μ_B), the experimental values are in agreement with an increase of the mean oxidation state of chromium in the "PbBi" compound. However, in both cases, they remain lower than those expected for pure spin contribution; this difference may be due to remaining magnetic interactions.

The study of the transport properties of these oxides shows that the chromium ones are insulators as expected, whereas the cobalt ones are semiconductors or poor metals (Fig. 11). The $\rho(T)$ curves of the cobalt phases show that for the "BiCaCo" oxide, the electrical resistivity (Fig. 11a) fits well the expression for activated transport $\rho = \rho_0 \exp(E_a/kT)$ with $E_a = 17$ meV, whereas for the "BiSrCo" samples (Figs. 11b–11c), it was not possible to satisfy this expression, reasonable agreement being obtained from variable range hopping mechanism $\rho = \rho_0 \exp(Q/T)^{1/4}$. In contrast, for the "BiPbSrCo" oxide the electrical resistivity seems to be close to that of "dirty" metal (Fig. 11d) as observed for the misfit layer oxides $Tl_x[(Sr_{1-y}Ca_y)O]_{1+x}CoO_2$ (4, 5). For this compound, at high temperature ($T > 80$ K) the resistivity increases with temperature with $d\rho/dT \approx 1.3\,10^{-4}\,\Omega\,cm\,K^{-1}$ for $T > 140$ K. At low temperature ($T < 60$ K) a localization of the charge carriers appears as shown by a negative value of $d\rho/dT$. In this range of temperature fits the expression $\rho = \rho_0 \exp(E_a/kT)$ with $E_a \approx 0.4$ meV. This value is one order of magnitude lower than that calculated in $Tl_{0.17}[Ca_{0.74}O]_{1.20}CoO_2$ (5).

CONCLUDING REMARKS

In this study, misfit layered oxides involving double rock salt layers, i.e., triple "AO", layers have been isolated for the first time. These compounds must be considered as the members "$m = 1/n = 3$" of a large family with generic formula $Bi_x[(A, Bi)_1 O)]_{n+nx/2}[MO_2]_m$ where $A = Ca$, Sr and $M = Co$, Cr. In this respect the thallium-based oxide $Tl_x(Sr_{0.9}O)_{1.12}CoO_2$ previously isolated represents the member "$m = 1/n = 2$" of this family. A tremendous, amount of work remains to be done to discover the other members of this series and to understand the possible nonstoichiometry, such as cation deficiency in the "AO" layers. In the same way, adequate substitutions should allow attractive magnetic and transport properties to be induced in these materials.

REFERENCES

1. J. Rouxel, *C. R. Acad. Sci. Paris* **323** (2b), 41 (1996).
2. G. A. Wieger and A. Meerschault, *J. Alloys Compounds* **178,** 351 (1992).
3. E. Makovicky and B. G. Hyde, *Struct. Bonding* **46,** 11 (1981).
4. Ph. Boullay, B. Domenges, M. Hervieu, D. Groult, and B. Raveau, *Chem. Mater.* **8,** 1482 (1996).
5. Ph. Boullay, R. Seshadri, F. Studer, M. Hervieu, D. Groult, and B. Raveau, *Chem. Mater.* **10,** 92 (1998).
6. J. Rodriguez-Carvajal, *In* "Satellites Meeting on Powder Diffraction," Abstracts of the XVth Conference on the International Union of Crystallography. p. 127. Toulouse, France, 1990.
7. C. Martin, M. Huve, M. Hervieu, A. Maignan, C. Michel, and B. Raveau, *Physica C*, **201,** 362 (1992).
8. H. W. Zandbergen, G. Van Tendeloo, J. Van Landuyt, and S. Amelinckx, *Appl. Phys. A* **46,** 233 (1988).
9. S. Kuypers, J. Van Landuyt, and S. Amelinckx, *J. Solid State Chem.* **86,** 212 (1990).
10. P. Conflant, J. C. Boivin, and D. J. Thomas, *J. Solid State Chem.* **35,** 192 (1980).
11. P. Conflant, J. C. Boivin, and D. J. Thomas, *J. Solid State Chem.* **18,** 133 (1976).
12. T. A. M. Haemers, D. J. W. Ijdo, and R. B. Helmholdt, *Mater Res. Bull* **27,** 1243 (1992).
13. I. N. Sora, W. Wong NG, Q. Huang, R. S. Roth, C. J. Brown, B. P. Burton, and A. Santoro, *J. Solid State Chem.* **109,** 251 (1994).
14. R. B. Helmholdt and D. J. W. Ijdo, *Mater. Res. Bull.* **26,** 989 (1991).
15. J. B. Parise, C. C. Torardi, C. J. Rawn, R. S. Roth, B. P. Burton, and A. Santoro, *J. Solid State Chem.* **102,** 132 (1993).